

MIT Open Access Articles

Strong Electronic Coupling of Molecular Sites to Graphitic Electrodes via Pyrazine Conjugation

The MIT Faculty has made this article openly available. **Please share** how this access benefits you. Your story matters.

Citation: Jackson, Megan N. et al. "Strong Electronic Coupling of Molecular Sites to Graphitic Electrodes via Pyrazine Conjugation." *Journal of the American Chemical Society* 140, 3 (January 2018): 1004–1010 © 2017 American Chemical Society

As Published: <http://dx.doi.org/10.1021/jacs.7b10723>

Publisher: American Chemical Society (ACS)

Persistent URL: <http://hdl.handle.net/1721.1/119426>

Version: Author's final manuscript: final author's manuscript post peer review, without publisher's formatting or copy editing

Terms of Use: Article is made available in accordance with the publisher's policy and may be subject to US copyright law. Please refer to the publisher's site for terms of use.



Strong electronic coupling of molecular sites to graphitic electrodes via pyrazine conjugation

Megan N. Jackson[†], Seokjoon Oh[†], Corey J. Kaminsky[†], Sterling B. Chu[†], Guanghui Zhang[‡], Jeffrey T. Miller^{‡§}, and Yogesh Surendranath[†]

[†] Department of Chemistry, Massachusetts Institute of Technology, Cambridge, Massachusetts 02139, United States

[‡] Davidson School of Chemical Engineering, Purdue University, West Lafayette, Indiana 47907, United States

[§] Chemical Science and Engineering Division, Argonne National Laboratory, Argonne, Illinois 60439, United States

KEYWORDS. *Electron transfer, outer-sphere, inner-sphere, surface immobilization, heterogeneous catalysis, tether, electrochemistry, cyclic voltammetry, X-ray absorption spectroscopy*

ABSTRACT: Glassy carbon electrodes were functionalized with redox-active moieties by condensation of *o*-phenylenediamine derivatives with *o*-quinone sites native to graphitic carbon surfaces. Electrochemical and spectroscopic investigations establish that these graphite-conjugated catalysts (GCCs) exhibit strong electronic coupling to the electrode, leading to electron transfer (ET) behavior that diverges fundamentally from that of solution phase or surface-tethered analogues. We find that: (1) ET is not observed between the electrode and a redox-active GCC moiety regardless of applied potential. (2) ET is observed at GCCs *only* if the interfacial reaction is ion-coupled. (3) Even when ET is observed, the oxidation state of a transition metal GCC site remains unchanged. From these observations, we construct a mechanistic model for GCC sites in which ET behavior is identical to that of catalytically active metal surfaces rather than to that of molecules in solution. These results suggest that GCCs provide a versatile platform for bridging molecular and heterogeneous electrocatalysis.

Introduction

The efficient interconversion of electrical and chemical energy requires catalysts capable of accelerating complex multi-electron reactions at electrified interfaces. These reactions can be carried out at the metallic surface sites of heterogeneous electrocatalysts or via redox mediation at molecular electrocatalysts. Molecular catalysts are straightforward to tune synthetically and characterize spectroscopically, allowing for unparalleled insight into their mechanisms of action. Similar molecular-level insight into metallic heterogeneous catalysts would be valuable not only on a fundamental level, but also on a practical level since these catalysts are commonplace in nearly all contemporary energy conversion devices, including fuel cells and electrolyzers. However, it is difficult, if not impossible, to obtain this level of understanding for most heterogeneous catalysts because surface active sites are inherently dynamic, difficult to modify at the molecular level, and hard to identify, much less characterize. Thus, advances in electrocatalysis require new strategies for controlling the surface reactivity of complex metallic heterogeneous interfaces at the molecular level.

Efforts toward molecular control of interfacial reactivity have largely centered on immobilizing molecular redox sites onto electrodes. A variety of methods have been developed for attaching molecules to conductive surfaces, including thiol-based self-assembled monolayers,^{1–3} diazonium grafts,^{4,5} click chemistry,^{6,7} alkynyl linkages,⁸ and noncovalent linkages that rely on

π - π interactions.⁹ However, these linkages provide relatively poor electron coupling between the appended units and the metallic electrode surface. For example, detailed studies on ferrocene-appended thiol SAMs display ET kinetics, including solvent reorganization energies and electron tunneling pre-factors, that are in line with outer-sphere ET as described by Marcus theory, suggesting that there is a tunneling barrier to ET in these systems.³ Thus the electrochemical and catalytic behavior of the tethered molecule closely resembles that of the dissolved species, not a metallic heterogeneous surface site.

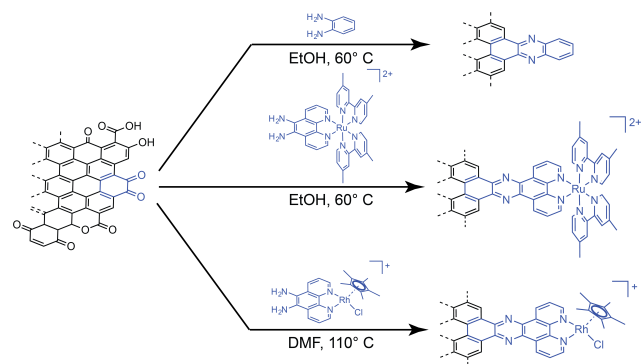
We have developed a simple method for linking molecules to graphitic carbon electrodes through conjugated aromatic pyrazine linkages. We have shown that *o*-phenylenediamine derivatives condense irreversibly with *o*-quinone moieties found natively at edge planes and step-edge defects of graphitic carbons to generate robust conjugated pyrazine linkages between the appended molecule and the surface.^{10,11} The resulting graphite conjugated catalysts (GCCs) are active for oxygen reduction in alkaline aqueous media.¹⁰ Additionally, GCCs bearing a Re coordination compound are active catalysts for the selective reduction of CO₂ to CO.¹¹

Herein, we show that these conjugated linkages lead to strong electronic coupling of the GCC sites to the graphitic electrode that dramatically alters their electrochemical behavior relative to solution-phase or surface-tethered molecular analogues. Electrochemical and X-ray absorption spectroscopy reveal that:

(1) Classical outer-sphere ET is not observed between the electrode and the GCC sites. (2) ET is observed at GCCs if the interfacial reaction is *ion-coupled*. (3) Even when ET is observed, the oxidation state of a transition metal GCC site remains unchanged. From these observations, we infer that GCC sites do not behave like their molecular analogues, but rather as metallic active sites with molecular definition. Consequently, GCCs form a unique class of materials that combines the high structural fidelity and tunability of molecular catalysts with the electronic properties of metallic extended solids.

Results

Scheme 1. Synthesis of GCC-phenazine (top), GCC-Ru (middle), and GCC-Rh (bottom).



Synthesis and characterization of GCCs

Chemically modified electrodes were prepared via treatment of carbon surfaces with phenylenediamine-containing precursors (**Scheme 1**) using procedures described previously (full synthetic details of electrode preparation are provided in the Supporting Information).¹⁰ Following surface treatment, modified electrodes were washed with ethanol and water, and soaked in 0.1 M HClO₄ to remove monoamine-linked and physisorbed species. X-ray photoelectron spectroscopy (XPS) and N K-edge X-ray absorption near edge structure (XANES) spectroscopy establish that this procedure selectively generates pyrazine linkages on graphitic carbon surfaces.¹⁰ Whereas GCC-phenazine electrodes were prepared by treating glassy carbon with *o*-phenylenediamine, GCC-Ru and GCC-Rh electrodes were prepared by treating glassy carbon with [Ru^{II}(dmbpy)₂(phenda)]²⁺ (dmbpy = 4,4'-dimethyl-2,2'-bipyridine, phenda = 5,6-diamino-1,10-phenanthroline) and [Rh^{III}Cp*(phenda)Cl]⁺ (Cp* = pentamethylcyclopentadienyl), respectively.

XPS data establish the fidelity of the primary coordination environments about the Ru and Rh centers in GCC-Ru and GCC-Rh, respectively. Survey XPS scans of GCC-Ru reveal a Ru:N ratio of approximately 1:7 (**Figure S1**), and survey scans of GCC-Rh reveal a Rh:N:Cl ratio of 1:4:1 (**Figure S2**), consistent with the 1:8 Ru:N and 1:4:1 Rh:N:Cl ratios expected of the conjugated species. High-resolution N 1s XPS of GCC-Ru is best fit to two peaks at 399.6 and 398.2 eV in a 3.5:1 ratio (**Figure S3**), in line with values expected for metal-bound pyridinic N and pyrazinic N, respectively.^{10,12} High-resolution N 1s XPS on GCC-Rh is best fit to two peaks in a 1:1 ratio at 399.9 and 399.0 eV (**Figure S4**), again consistent with the expected binding energies for metal-bound pyridinic N and pyrazinic N.

Together, these data suggest that GCC-Ru and GCC-Rh surfaces contain a uniform array of [Ru^{II}(dmbpy)₂(phen)]²⁺ (phen = 1,10-phenanthroline) and [Rh^{III}Cp*(phen)Cl]⁺ moieties conjugated to glassy carbon electrodes through pyrazine linkages.

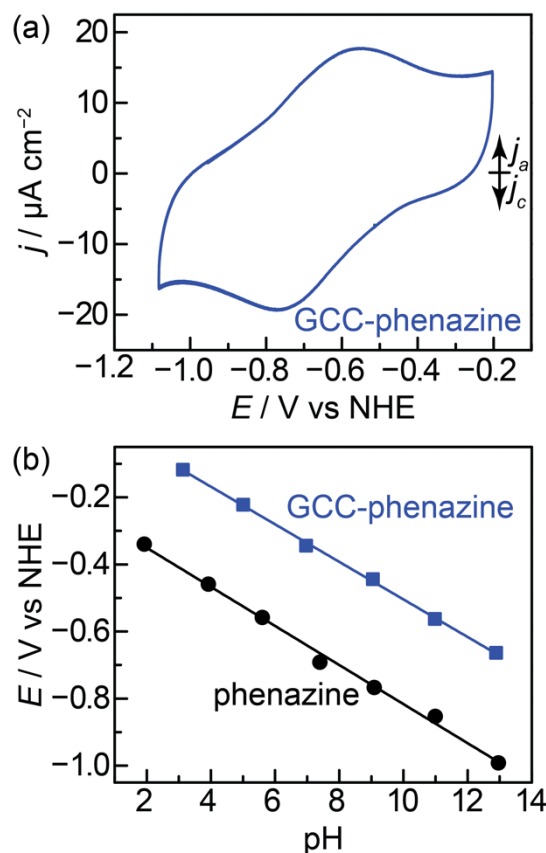


Figure 1. (a) Cyclic voltammogram (10 mV s⁻¹) of GCC phenazine recorded in 0.1 M NaOH. (b) $E_{1/2}$ vs pH for dissolved phenazine (red) and GCC-phenazine (black). Values for dissolved phenazine are re-plotted from literature values obtained from linear sweep voltammograms recorded in 10% ethanolic aqueous electrolyte.¹³ CVs of GCC phenazine were recorded at 10 mV s⁻¹ in pH-adjusted 0.1 M borate/0.1 M phosphate/0.1 M formate aqueous electrolyte.

Electrochemistry of GCC-phenazine

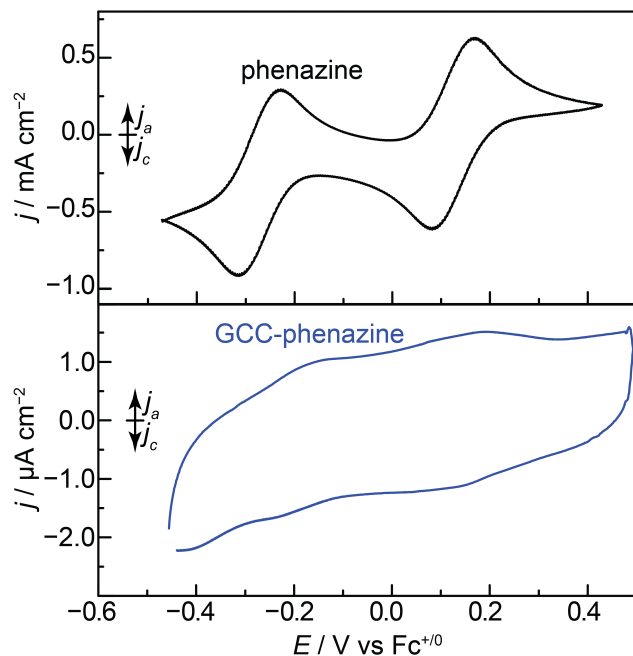


Figure 2. CVs of dissolved phenazine (5 mM, 100 mV s^{-1}) (top) and GCC-phenazine (10 mV s^{-1}) (bottom) recorded in acetonitrile electrolyte containing 0.1 M TBAPF₆ and 0.2 M tosylic acid.

In protic electrolytes, the electrochemical response arising from GCC-phenazine is similar to that of molecular phenazine. In aqueous electrolyte, phenazine undergoes a two-proton, two-electron reduction to dihydrophenazine at $E_{1/2} = -0.23$ V vs RHE.¹³ Similarly, at pH 13, cyclic voltammograms (CVs) of GCC-phenazine reveal a broad reversible wave at $E_{1/2} = 0.12$ V vs RHE (-0.65 V vs NHE, **Figure 1a**). Despite the relatively slow scan rate, this surface wave displays a large peak-to-peak separation of 220 mV at 10 mV s^{-1} , indicative of a slow charge transfer process on the surface. The $E_{1/2}$ of these redox waves shift in a roughly Nernstian fashion by 58 and 56 mV per pH unit for phenazine and GCC-phenazine, respectively (**Figures 1b** and **S5**),¹³ suggesting that both processes are proton-coupled reactions involving an equal number of protons and electrons. Similarly, in acetonitrile electrolyte containing 0.1 M tetrabutylammonium hexafluorophosphate (TBAPF₆) and 0.2 M tosylic acid, CVs of phenazine display two reversible redox waves at $E_{1/2} = -0.29$ V and 0.10 V vs Fc^{+/0}, attributed to two sequential one-proton, one-electron transfer processes (**Figure 2**, top),¹⁴ and CVs of GCC-phenazine display two analogous, albeit broad, redox features at -0.19 V and 0.14 V (**Figure 2**, bottom). This broadness is not due to significant degradation of the surface linkage. CVs recorded in water following cycling in acetonitrile with tosylic acid reveal well-defined waves of similar magnitude (**Figure S6**). Instead, we attribute this broadness to the known sluggishness of interfacial PCET in acetonitrile versus water.^{15,16} Together, these data indicate that in protic electrolytes, both surface-bound GCC-phenazine units and dissolved molecular phenazines undergo chemically reversible proton-coupled ET reactions.

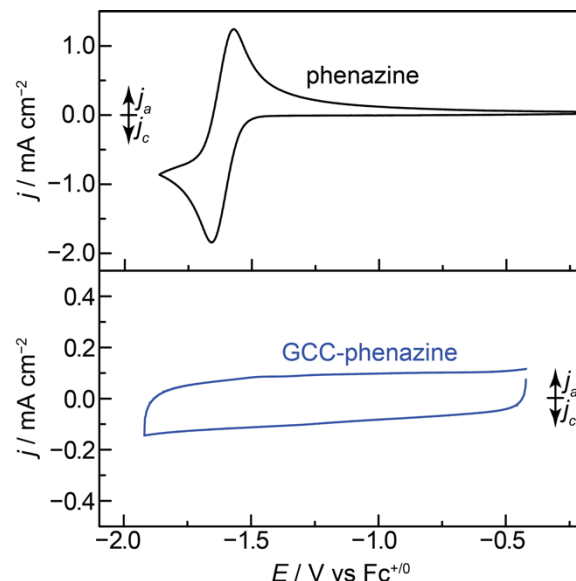


Figure 3. CVs of dissolved phenazine (5 mM, 100 mV s^{-1}) (top) and GCC-phenazine (10 mV s^{-1}) (bottom) recorded in acetonitrile electrolyte containing 0.1 M TBAPF₆.

While phenazine and GCC-phenazine display similar redox behavior in protic electrolytes, they display radically different electrochemical behavior in the absence of a proton donor. In acetonitrile electrolyte containing 0.1 M TBAPF₆ and no acid, dissolved phenazine displays a reversible one-electron redox wave at $E_{1/2} = -1.61$ V vs Fc^{+/0} (**Figure 3**, top); however, GCC-phenazine electrodes display no discernible redox features beyond the background double-layer charging current (**Figure 3**, bottom). Importantly, redox features are not observed even upon scanning to the solvent window (**Figure S7**), increasing the electrolyte strength from 0.1 M to 0.5 M TBAPF₆ (**Figure S8**), exchanging Li⁺ for TBA⁺ (**Figure S9**), exchanging Cl⁻ for PF₆⁻ (**Figure S10**), or varying the scan rate between 100 mV s^{-1} and 10 mV s^{-1} (**Figure S11**). In short, unlike its molecular analogue, GCC-phenazine electrodes only give rise to discernable redox waves in protic electrolytes.

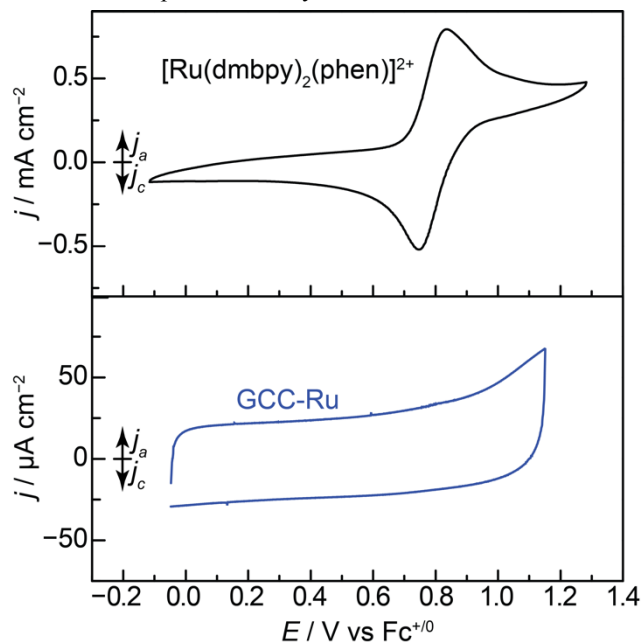


Figure 4. CVs of dissolved $[\text{Ru}^{\text{II}}(\text{dmbpy})_2(\text{phen})]^{2+}$ (5mM, 100 mV s^{-1}) (top) and GCC-Ru (10 mV s^{-1}) (bottom) recorded in acetonitrile electrolyte containing 0.1 M TBAPF₆.

Electrochemistry of GCC-Ru

We now analyze the electrochemical behavior of metal-containing GCCs in comparison to soluble analogs. In solution, $[\text{Ru}^{\text{II}}(\text{dmbpy})_2(\text{phen})]^{2+}$ undergoes a chemically reversible, outer-sphere one-electron transfer at $E_{1/2} = 0.79 \text{ V vs Fc}^{+/0}$, which we assign to the $\text{Ru}^{\text{III/II}}$ couple (**Figure 4**, top). This metal-based outer-sphere ET is not observed for GCC-Ru electrodes. Instead, only background double layer charging current is observed in the potential region over which the dissolved molecule is oxidized with the onset of the solvent window at $\sim 0.9 \text{ V}$ (**Figure 4**, bottom). While this solvent window rises earlier than that of the unfunctionalized electrode, the magnitude of the current is strongly dependent on the trace water concentration in the acetonitrile electrolyte and decreases with increasing scan rate. Together, these observations lead us to postulate that this current arises from slow reaction with adventitious water and is unrelated to outer sphere Ru oxidation. As above, we do not observe reversible redox features for GCC-Ru upon increasing the electrolyte strength from 0.1 M TBAPF₆ to 0.5 M TBAPF₆ (**Figure S12**), exchanging TBA^+ for Li^+ (**Figure S13**), or varying the scan rate between 100 mV s^{-1} and 10 mV s^{-1} (**Figure S14**). CVs of GCC-Ru recorded in 0.1 M HClO_4 after polarization in acetonitrile establish that the phenazine moiety remains intact (**Figure S15**). The amount of Ru remaining on the surface after polarization was determined by inductively coupled plasma mass spectrometry (ICP-MS) following acid digestion of the surface (see Supporting Information for details). Noting the two-electron stoichiometry of phenazine reduction, we find a Ru:phenazine surface concentration ratio of 0.9, indicating that the Ru surface sites remain intact on the surface over the course of the measurement. **Figure S15** compares the magnitude of the phenazine wave to the CV trace in **Figure 4** (bottom), indicating that, at these loadings, a surface $\text{Ru}^{\text{III/II}}$ redox wave, if it existed, would be easily discernable over background double layer charging current. Together, these data suggest that GCC-Ru sites, unlike soluble $[\text{Ru}^{\text{II}}(\text{dmbpy})_2(\text{phen})]^{2+}$, do not give rise to discrete surface charge transfer waves.

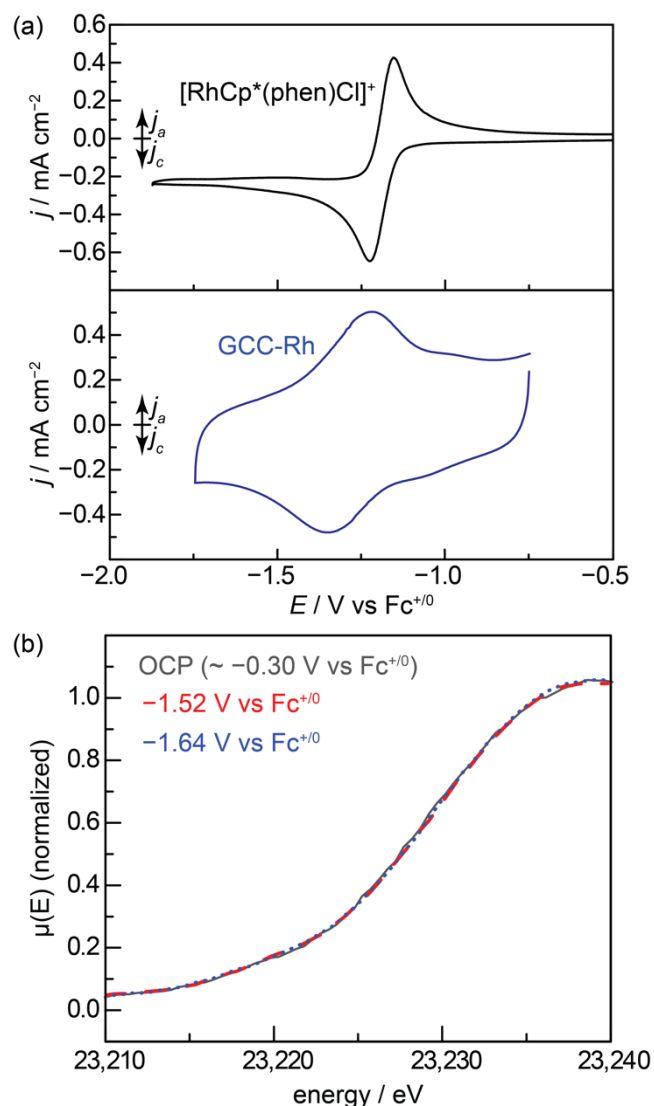


Figure 5. CVs of dissolved $[\text{Rh}^{\text{III}}\text{Cp}^*(\text{phen})\text{Cl}]^+$ (5 mM, 100 mV s^{-1}) (a, top) and GCC-Rh (10 mV s^{-1}) (a, bottom) recorded in acetonitrile electrolyte containing 0.1 M TBACl. (b) in situ Rh K-edge X-ray absorption near edge structure spectra of GCC-Rh recorded in acetonitrile electrolyte containing 0.1 M TBACl and held at the open circuit potential (OCP, $\sim -0.3 \text{ V}$), -1.43 V , and $-1.55 \text{ V vs Fc}^{+/0}$.

Electrochemistry and X-ray absorption spectroscopy of GCC-Rh

In order to examine the behavior of metal-containing GCCs that are able to undergo redox-induced ligand exchange, we compared the redox chemistry of GCC-Rh with its soluble analog $[\text{Rh}^{\text{III}}\text{Cp}^*(\text{phen})\text{Cl}]^+$. At $-1.19 \text{ V vs Fc}^{+/0}$, $[\text{Rh}^{\text{III}}\text{Cp}^*(\text{phen})\text{Cl}]^+$ undergoes two-electron reduction from Rh^{III} to Rh^{I} with simultaneous dissociation of the bound Cl^- ligand and (**Figure 5a**, top).^{17,18} The analogous GCC-Rh electrode displays a reversible redox wave at -1.29 V in 0.1 M TBACl in acetonitrile (**Figure 5a**, bottom). The electron stoichiometry of this wave was determined by integrating the charge in CVs of GCC-Rh in 0.1 M TBACl and comparing it to the amount of Rh on the surface as measured by acid digestion of the surface and ICP-MS quantification. Using this procedure, we measured an electron:Rh ratio of 1.01 (95% CI [0.74:1.28], see Supporting

Information for details). In TBABr and TBAI, the wave shifts by +60 mV and +40 mV (**Figure S16**), respectively, indicating the wave is sensitive to the identity of the halide. We assign the cathodic wave to dissociation of an inner-sphere halide and the anodic wave to reassociation of the majority halide in the electrolyte. This assignment is corroborated by XPS data that show a complete absence of Cl from the surface upon polarizing a GCC-Rh electrode in the presence of TBAPF₆ (**Figure S17**). Furthermore, the reversible wave observed in TBAX (X = Cl[−], Br[−], or I[−]) becomes chemically irreversible upon introduction of CO to the solution (**Figure S18**). Upon subsequent cycling of the electrode in CO, the wave disappears altogether. XPS spectra taken after polarizing in CO-saturated solution at −1.31 V vs Fc⁺⁰ show a N:Rh ratio of 4.6:1, suggesting that the Rh species remains in-tact in the presence of CO (**Figure S19**). We attribute the disappearance of the CV feature in this medium to the irreversible binding of CO to the Rh site upon halide dissociation, which prevents the Rh from reassociating Cl[−]. This attribution is consistent with the absence of Cl in the XPS, even after scanning back to −0.86 V vs Fc⁺⁰ (+0.34 V vs the GCC-Rh wave). Together, these data suggest that metal-based GCC sites can give rise to redox waves, provided that they are able to undergo ion exchange with the solution.

Notably, the GCC-Rh wave corresponds to a *one-electron* process, in contrast to the known two-electron process for the soluble Rh molecule. This discrepancy implies that the surface redox wave observed for GCC-Rh is distinct from the redox activity of the molecular species. To directly probe the valency of the GCC-Rh sites during the observed redox process, we monitored the oxidation state of Rh as a function of applied potential via in situ X-ray absorption near-edge structure (XANES) spectroscopy. Based on literature precedent, the reduction of Rh^{III} to Rh^I is expected to shift the rising portion of the K-edge to lower energy by 2–3 eV.^{19,20} Indeed, we observe a significant difference in both the position and shape of the K-edge between [Rh^{III}Cp*(phen)Cl]⁺ and Rh^ICp*(phen) (**Figure S20**). The Rh K-edge for [Rh^{III}Cp*(phen)Cl]⁺ has an inflection point at 23,226.5 eV, while the Rh K-edge for Rh^ICp*(phen) onsets earlier and has two inflection points at 23,225.6 and 23,231.7 eV (**Figure S21**). The different edge shapes are attributed to a difference in coordination number and geometry between the two compounds. We expect similar changes for complexes tethered to the surface through a non-conjugated insulating linker. While we were unable to collect in situ XANES data on the analogous aliphatically tethered [Rh^{III}Cp*(phen)Cl]⁺ complex due to the instability of the linkage under reductive polarization, in situ XANES data collected on electrodes modified with a noncovalently tethered [Ru^{II}(dmbpy)₂(bpy)]²⁺ (bpy = 2,2'-bipyridine) complex²¹ reveal a 0.7 eV shift in the Ru K-edge upon polarization at 1.1 V vs Fc⁺⁰ (0.3 V beyond the Ru^{III/II} wave) (**Figure S22**), exactly in line with the 0.7 eV shift observed between Ru^{II} and Ru^{III} model complexes (**Figure S23**). Remarkably, in situ XANES data collected on GCC-Rh samples at the open circuit potential (~−0.3 V vs Fc⁺⁰), 0.12 V negative of the GCC-Rh redox wave (−1.43 V vs Fc⁺⁰), and 0.24 V negative of the redox wave (−1.55 V vs Fc⁺⁰) are all identical (Rh K-edge of 23,229.0 eV) (**Figure 5b**), indicating that even though electrical polarization gives rise to current flow and halide dissociation, it does not lead to a detectable change in the oxidation state of Rh.

Mechanistic Model

The electrochemical and XAS studies described above establish that the redox chemistry of GCCs is radically different than that of dissolved molecular analogues. In particular, we observe that (1) GCCs display discrete redox features *only* when electron flow is coupled to ion-transfer at the interface, in analogy to metal surface sites, and (2) even during interfacial ion-coupled electron transfer, the oxidation state of the metal center undergoing ion exchange remains *unchanged*. These surprising observations form the basis for a mechanistic model in which molecules that are conjugated to graphite are *part of* the electrode rather than merely appended to it.

We first note that the absence of a clear redox feature for GCC-Ru and GCC-phenazine in aprotic electrolyte could result from the actual absence of charge transfer or from an extreme level of broadening of the surface wave so as to make it indistinguishable from the background double-layer charging current. Broadening could occur for several reasons, which we exclude in turn. First, interactions between neighboring surface sites have been shown to lead to wave broadening for a variety of chemically-modified electrodes;²² however, these effects are typically observed when there are strong interactions between the appended redox moieties. Although we cannot entirely exclude the presence of lateral interactions between GCC surface sites, the low coverage of phenazine groups on GCCs (~0.25 nmol cm^{−2})¹⁰ is comparable to that observed for dilute ferrocenyl mixed self-assembled monolayers which display un-broadened surface redox features.²² Thus, it is unlikely that the waves would broaden so significantly as to make them unobservable. Second, CV waves can appear broad when there is insufficient electrostatic screening. We exclude this explanation because CVs collected at 100 mM TBAPF₆ and 500 mM TBAPF₆ were identical, (**Figures S8 and S12**) and because no redox features were observed when TBA⁺ was replaced with Li⁺ (**Figures S9 and S13**) or when PF₆[−] was replaced with Cl[−] (**Figure S10**). Finally, CV waves can broaden due to kinetic sluggishness. We do not believe that the absence of redox waves for GCC-phenazine and GCC-Ru is due to kinetic sluggishness because our observations are independent of scan rate; despite varying the scan rate between 100 mV s^{−1} and 10 mV s^{−1}, we never observed redox features (**Figures S11 and S14**). Additionally, both phenazine and [Ru^{II}(dmbpy)₂(phen)]²⁺ exhibit rapid charge transfer kinetics; the reported outer-sphere electrochemical ET rate constants for phenazine and [Ru^{II}(phen)₃]²⁺ in acetonitrile are 2.0 × 10^{−2} cm s^{−1} and 1.7 cm s^{−1}, respectively.^{14,23} Indeed, we expect the conjugated linkage between the GCC site and the electrode to accelerate ET rates relative to electron tunneling through solvent. Most convincingly, the cases where we *do* observe GCC redox waves all involve ion transfer, and this additional nuclear motion would, if anything, slow the rate of the reaction relative to a simple outer-sphere ET. We conclude that the absence of redox features in GCC-phenazine and GCC-Ru in aprotic acetonitrile electrolyte is most likely because no ET is occurring.

It is possible that ET is not observed in these cases because the redox potential of the surface site has been shifted outside the solvent window and is no longer accessible. Indeed, the two-electron, two-proton redox feature observed for GCC-phenazine in aqueous electrolyte occurs ~200 mV positive of the reduction of phenazine in the same medium, and arguments based on electron-delocalization would lead us to predict a positive shift in nonaqueous electrolytes as well. However, while phenazine in acetonitrile electrolyte displays a redox feature at −1.61 V vs Fc⁺⁰, we do not observe a redox wave for GCC-

phenazine between -2.5 and 1.0 V vs $\text{Fc}^{+/0}$ (**Figure S7**). We believe that a shift in the $E_{1/2}$ of phenazine of > 2 V is unreasonable. Similarly, we would not expect a substantial change in the $\text{Ru}^{\text{III/II}}$ potential for $[\text{Ru}^{\text{II}}(\text{dmbpy})_2(\text{phen})]^{2+}$ upon conjugation. Replacing a dipyrro[3,2- a' :3',3'- c]phenazine ligand for 1,10-phenanthroline in pseudooctahedral Ru^{II} complexes has been shown to shift the $\text{Ru}^{\text{III/II}}$ potential to positive values by less than 0.03 V.^{24,25} For GCC-Ru, we do not observe a redox wave despite scanning > 0.35 V positive of the expected value, too large of a shift to be explained by changes in the π acidity of the surface-conjugated phenanthroline ligand. It follows that if no reversible redox wave is observed even 0.35 V past the expected E° , the variation in applied potential is not imposing a substantial driving force for ET to the Ru center.

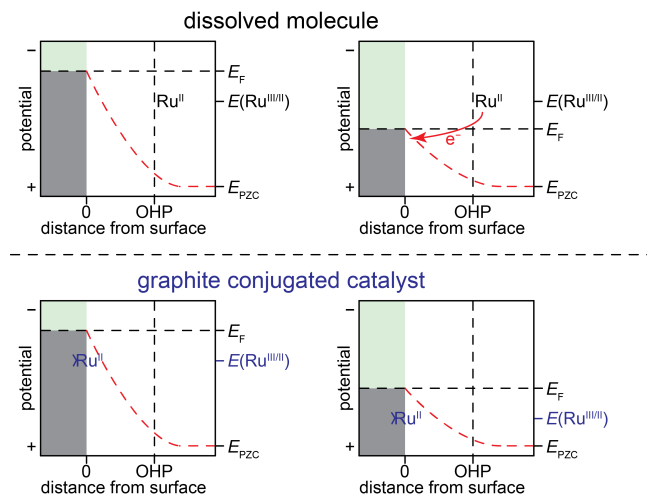


Figure 6. Putative interfacial free energy diagrams for unmodified electrodes with dissolved Ru^{II} molecules (top) and electrodes modified with conjugated Ru^{II} surface sites (bottom). The diagram denotes the Fermi level of the electrode, E_F , and the redox potential of the molecule, $E(\text{Ru}^{\text{III/II}})$, upon varying the applied potential (left to right). The electrostatic potential across the electrochemical double layer is indicated by the red dotted line. Varying E_F does not impact $E(\text{Ru}^{\text{III/II}})$ for the dissolved molecule, leading to classical outer-sphere ET (top) at the interface. For GCCs (bottom), varying E_F simultaneously shifts the energy levels of donor/acceptor states in the conjugated molecule by a similar magnitude, and the driving force for ET remains unchanged.

We attribute this unique behavior of GCCs to the nature of the pyrazine linkage. In the absence of a conjugated linkage, the driving force for outer sphere ET is given by the difference between the Fermi level of the electrode and the E^0 of the molecular species. As the potential is varied, the electrode is charged, causing a buildup of opposing charge near the electrode surface at the outer Helmholtz plane (OHP). This charge buildup at the interface establishes an electric field gradient, changing the Fermi level of the electrode relative to the energies of the molecular donor/acceptor states residing at or beyond the OHP (**Figure 6**, top). Thus, as the potential changes, the driving force for ET also changes.

The inability to do outer-sphere ET to GCC sites suggests that varying the potential does not lead to the same change in ET driving force for this conjugated system. This lack of driving force is consistent with double-layer theory if and only if the molecular fragment is electronically coupled to the electrode. In metallic electrodes, the metal atoms are strongly coupled to the

band states of the solid, and the effective conductivity of a metal ensures that the Fermi level of the surface-exposed metal atoms is identical to that of the bulk. Upon application of a potential, the ensuing interfacial field gradient raises the Fermi level of the solid *and* the energy levels of surface atoms in synchrony; thus, the energy separation between the donor/acceptor states of the surface atoms and the Fermi level remain the same irrespective of the applied potential.²⁶ Our data indicate that the same phenomenon is occurring in GCCs. In particular, the inability to observe outer-sphere ET in GCCs indicates that the pyrazine linkage electronically couples the molecular fragment to the electrode. This electronic coupling ensures that the separation between the Fermi level of the carbon and the molecular donor/acceptor states of the appended fragments remain largely invariant with applied potential; i.e., varying the applied potential does not change the *difference* in the potential between the electrode and the GCC site, thereby eliminating the possibility of outer-sphere ET between them (**Figure 6**, bottom).

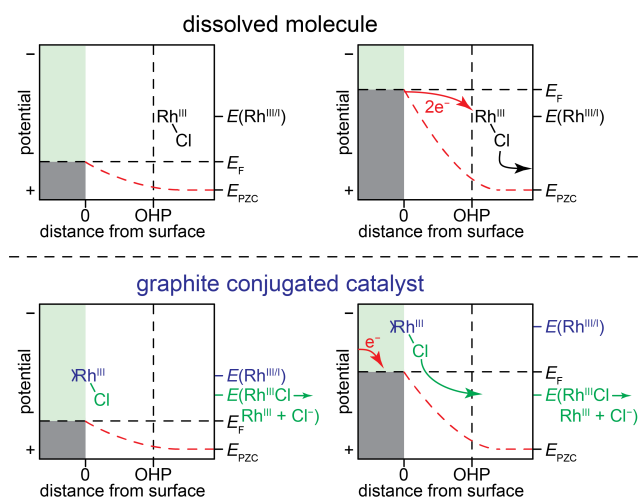


Figure 7. Putative interfacial free energy diagrams for unmodified electrodes with dissolved $\text{Rh}^{\text{III}}\text{-Cl}$ molecules (top) and electrodes modified with conjugated $\text{Rh}^{\text{III}}\text{-Cl}$ surface sites (bottom). The diagram denotes the Fermi level of the electrode, E_F , upon varying the applied potential (left to right) as well as the redox potential of the molecule, $E(\text{Rh}^{\text{III/II}})$, and the potential for halide dissociation from the surface $E(\text{Rh}^{\text{III}}\text{-Cl} / \text{Rh}^{\text{III}} + \text{Cl}^-)$. The electrostatic potential across the electrochemical double layer is indicated by the red dotted line. Varying E_F drives two-electron transfer to Rh via interfacial outer-sphere ET (top). For GCCs (bottom), varying E_F shifts the electrostatic potential of the surface, driving halide dissociation, while simultaneously shifting the energy levels of the Rh acceptor states, preventing Rh-centered reduction.

Even though our data suggest that there is negligible potential drop between the electrode and the GCC site, there is a potential drop between the GCC site and the solution. Therefore, varying the applied potential can alter the driving force for *ions* to transfer between the GCC site and the solution, provided that the surface site is able to bind the ion in question. Our data suggest that this is occurring for GCC-phenazine in protic media and GCC-Rh in halide electrolytes. In protic electrolyte, the N sites on the phenazine unit of GCC-phenazine can form and break bonds with protons. When the applied potential is sufficiently negative, the electric field drives protons to cross the double layer and bind to the N sites. Since protons carry a positive

charge, compensating electrons must flow from the external circuit in order to maintain the electrode potential.²⁶ This compensatory current is observed as a surface redox wave (**Figures 1a** and **2**, bottom). Since all N sites are expected to bind protons with similar affinity, ET occurs over a relatively narrow potential range, leading to a distinct wave above the background double-layer charging current.

Similarly, the Rh in GCC-Rh binds a Cl^- ion, and when the potential is sufficiently negative, the electric field drives this negatively charged ion across the double layer into solution. Again, this ion dissociation leads to compensatory electron flow from the external circuit, which we observe as a redox wave (**Figure 5a**, bottom). A model for this behavior is depicted in **Figure 7**, bottom, in which the E^0 at which Cl^- dissociates is denoted as $E(\text{Rh}^{\text{III}}\text{Cl} \rightarrow \text{Rh}^{\text{III}} + \text{Cl})$ and does not vary with the potential applied at the electrode. Importantly, in this model, only the exchange of specifically adsorbed ions gives rise to redox features, consistent with our observation of a 1 e^- stoichiometry in the wave. This model is also consistent with the observed chemical irreversibility of the GCC-Rh wave in the presence of CO. We postulate that the strong binding affinity of CO with Rh leads to the irreversibility by preventing the re-association of the halide.

Perhaps even more surprisingly, the in situ XANES data (**Figure 5b**) indicate that the oxidation state of the Rh remains constant throughout the redox event for GCC-Rh, suggesting that a change in site valency is not necessary for charge transfer from the external circuit. This observation is particularly interesting because if the electron is not going to the metal, it raises the question, “Where is the electron going?” The answer, of course, is the ligand, and for a GCC, the ligand is the carbon electrode itself. Indeed, the metallic band structure of graphitic carbon makes it redox non-innocent in the extreme. We can therefore write the following equilibrium to describe the charge transfer wave observed for GCC-Rh (**Figure 8**):

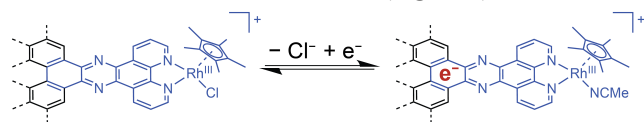


Figure 8. Proposed balanced reaction for the redox wave observed at $-1.29\text{ V vs Fc}^{+/0}$. The red “ e^- ” represents an electron residing in a graphite-centered band state of the solid and is drawn in this particular ring symbolically.

in which the applied potential drives dissociation of the inner-sphere halide with electron flow to a graphite ligand-centered band state of the solid. Although we do not have a direct spectroscopic probe of the coordination sphere of the product, we postulate that acetonitrile binds to the Rh upon halide dissociation to complete its coordination sphere. Nonetheless, the reaction described in **Figure 8** is consistent with the invariance of the oxidation state at the Rh center upon polarization beyond the redox wave.

The behavior of the Rh sites in GCC-Rh is consistent with the model for GCC-Ru (**Figure 6**), and is captured in **Figure 7**. Just as varying the potential at a GCC-Ru electrode simultaneously shifts the energies of the Ru orbitals, varying the potential at a GCC-Rh electrode simultaneously shifts the energy of the Rh orbitals. In both cases, the metal site remains in electrostatic equilibrium with the graphite electrode regardless of the applied potential, and metal-centered oxidation or reduction does not

occur. Consequently, ion-transfer to GCC sites occurs with coincident ET to carbon-based orbitals.

The reactivity patterns of GCCs mimic those of metallic surface sites. At metal surface sites, ET proceeds exclusively via inner-sphere mechanisms in which electron flow is driven by ions or molecules crossing the double layer. As a result, ET is only observed when bonds are made or broken at metallic surface sites, and no ET occurs in the absence of a species that is able to adsorb to the surface. Our data suggest that ET at graphite-conjugated molecules also proceeds exclusively via inner-sphere pathways, making GCCs mechanistically indistinguishable from authentic metallic surfaces.

Conclusion

The mechanistic studies described above suggest that GCCs are a unique class of materials that combines the high structural fidelity and tunability of molecular catalysts with the electronic properties of metallic extended solids. We attribute this unique behavior of GCCs to the conductive aromatic linkage that provides for sufficiently strong electronic coupling such that there is negligible potential drop between the electrode and the GCC site. Furthermore, we show that the oxidation state of GCC sites can remain constant throughout a redox event. Thus, the valency and reduction potential of the molecular analogue do not directly dictate the rate and driving force for elementary and catalytic redox reactions at GCCs. Instead, redox chemistry at GCCs is driven by the binding strength of substrates and intermediates with the surface sites. These unique characteristics of GCCs make their ET behavior indistinguishable from that of surface sites at metallic heterogeneous catalysts.

Due to their metal-like behavior, GCCs provide a versatile platform with which to probe heterogeneous electrochemical reactivity at the molecular level. Spectroscopic studies of active sites on bulk or nanoscopic metal electrocatalysts are difficult if not impossible in many cases because the signal from the active sites is dwarfed by a substantial bulk background. Moreover, even surface-sensitive techniques provide signals that reflect the ensemble average behavior of both active and spectator surface sites. As exemplified by the in situ XANES experiments reported here, GCCs overcome this limitation, enabling molecular-level investigations into the thermochemistry and kinetics of both elementary and catalytic electrochemical reactions that form the basis for important energy conversion technologies.

ASSOCIATED CONTENT

Supporting Information. Full experimental details, synthetic details, ICP-MS data, XPS data, and additional CVs and XAS data. This material is available free of charge via the Internet at <http://pubs.acs.org>.

AUTHOR INFORMATION

Corresponding Author

* yogi@mit.edu

ACKNOWLEDGMENTS

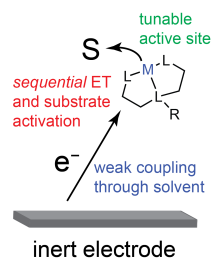
We gratefully acknowledge A. Jeremy Kropf and Joshua Wright for assistance with the XAS experiments. We acknowledge Christopher E. D. Chidsey and Richard L. McCreery for helpful discussions. This research was supported by the U.S. Department of Energy, Office of Science, Office of Basic Energy Sciences, under

award number DE-SC0014176. M.N.J. is supported by the Department of Defense (DoD) through the National Defense Science & Engineering Graduate Fellowship (NDSEG) Program. S.O. and C.J.K. were supported by the National Science Foundation Graduate Research Fellowship under Grant No. 1122374. Use of the Advanced Photon Source is supported by the U.S. Department of Energy, Office of Science, and Office of Basic Energy Sciences, under Contract DE-AC02-06CH11357. MRCAT operations are supported by the Department of Energy and the MRCAT member institutions. XPS investigations made use of Shared Experimental Facilities supported in part by the MRSEC Program of the National Science Foundation under award no. DMR-1419807. Support for ICP-MS investigations was provided by a core center grant P30-ES002109 from the National Institute of Environmental Health Sciences, National Institutes of Health.

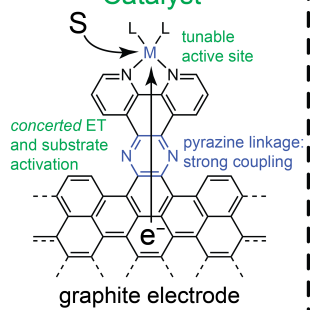
REFERENCES

- (1) Love, J. C.; Estroff, L. A.; Kriebel, J. K.; Nuzzo, R. G.; Whitesides, G. M. *Chem. Rev.* **2005**, *105*, 1103.
- (2) Beulen, M. W. J.; Kastenberger, M. I.; van Veggel, F. C. J. M.; Reinhoudt, D. N. *Langmuir* **1998**, *14*, 7463.
- (3) Chidsey, C. E. *Science* **1991**, *251*, 919.
- (4) Pinson, J.; Podvorica, F. *Chem. Soc. Rev.* **2005**, *34*, 429.
- (5) Mahouche-Chergui, S.; Gam-Derouich, S.; Mangeney, C.; Chehimi, M. M. *Chem. Soc. Rev.* **2011**, *40*, 4143.
- (6) McCrory, C. C. L.; Devadoss, A.; Ottenwaelder, X.; Lowe, R. D.; Stack, T. D. P.; Chidsey, C. E. D. *J. Am. Chem. Soc.* **2011**, *133*, 3696.
- (7) Devadoss, A.; Chidsey, C. E. D. *J. Am. Chem. Soc.* **2007**, *129*, 5370.
- (8) Sheridan, M. V.; Lam, K.; Geiger, W. E. *J. Am. Chem. Soc.* **2013**, *135*, 2939.
- (9) Blakemore, J. D.; Gupta, A.; Warren, J.; Brunschwig, B. S.; Gray, H. B. *J. Am. Chem. Soc.* **2013**, *135*, 18288.
- (10) Fukushima, T.; Drisdell, W.; Yano, J.; Surendranath, Y. *J. Am. Chem. Soc.* **2015**, *137*, 10926.
- (11) Oh, S.; Gallagher, J. R.; Miller, J. T.; Surendranath, Y. *J. Am. Chem. Soc.* **2016**, *138*, 1820.
- (12) Brisdon, B. J.; Griffin, G. F.; Pierce, J.; Walton, R. A. *J. Organomet. Chem.* **1981**, *219*, 53.
- (13) Kaye, R. C.; Stonehill, H. I. *J. Chem. Soc.* **1952**, 3240.
- (14) Sawyer, D. T.; Komai, R. Y. *Anal. Chem.* **1972**, *44*, 715.
- (15) Jackson, M. N.; Surendranath, Y. *J. Am. Chem. Soc.* **2016**, *138*, 3228.
- (16) Bonin, J.; Costentin, C.; Louault, C.; Robert, M.; Savéant, J.-M. *J. Am. Chem. Soc.* **2011**, *133*, 6668.
- (17) Caix, C.; Chardon-Noblat, S.; Deronzier, A.; Ziessel, R. *J. Electroanal. Chem.* **1993**, *362*, 301.
- (18) Chardon-Noblat, S.; Cosnier, S.; Deronzier, A.; Vlachopoulos, N. *J. Electroanal. Chem.* **1993**, *352*, 213.
- (19) Cipot-Wechsler, J.; Covelli, D.; Praetorius, J. M.; Hearn, N.; Zenkina, O. V.; Keske, E. C.; Wang, R.; Kennepohl, P.; Crudden, C. M. *Organometallics* **2012**, *31*, 7306.
- (20) Desnoyer, A. N.; Behyan, S.; Patrick, B. O.; Dauth, A.; Love, J. A.; Kennepohl, P. *Inorg. Chem.* **2016**, *55*, 13.
- (21) Gupta, A.; Blakemore, J. D.; Brunschwig, B. S.; Gray, H. B. *J. Phys. Condens. Matter* **2016**, *28*, 94002.
- (22) Chidsey, C. E. D.; Bertozzi, C. R.; Putvinski, T. M.; Muijsce, A. M. *J. Am. Chem. Soc.* **1990**, *112*, 4301.
- (23) Winkler, K.; McKnight, N.; Fawcett, W. R. *J. Phys. Chem. B* **2000**, *104*, 3575.
- (24) Kobayashi, K.; Ohtsu, H.; Nozaki, K.; Kitagawa, S.; Tanaka, K. *Inorg. Chem.* **2016**, *55*, 2076.
- (25) Lever, A. B. P. *Inorg. Chem.* **1990**, *29*, 1271.
- (26) Schmickler, W.; Santos, E. *Interfacial electrochemistry*; 2010.

Molecular Catalyst



Graphite-Conjugated Catalyst



Heterogeneous Catalyst

